

PHASES: a concept for a satellite-borne ultra-precise spectrophotometer

C. del Burgo^{a,b,*}, C. Allende Prieto^c and T. Peacocke^d

^a *UNINOVA-CA3, Campus da Caparica, Quinta da Torre, Monte de Caparica 2825-149, Caparica, Portugal*

^b *School of Cosmic Physics, Dublin Institute for Advanced Studies, Dublin 2, Ireland*

^c *Mullard Space Science Laboratory, University College London, Holmbury St. Mary, Dorking, Surrey RH5 6NT, United Kingdom*

^d *Experimental Physics, National University of Ireland, Maynooth, Co. Kildare, Ireland*

ABSTRACT: The *Planet Hunting and Asteroseismology Explorer Spectrophotometer*, PHASES, is a concept for a space-borne instrument to obtain flux calibrated spectra and measure micro-magnitude photometric variations of nearby stars. The science drivers are the determination of the physical properties of stars and the characterisation of planets orbiting them, to very high precision. PHASES, intended to be housed in a micro-satellite, consists of a 20 cm aperture modified Baker telescope feeding two detectors: the tracking detector, with a field of 1 degree square, and the science detector for performing spectrophotometry. The optical design has been developed with the primary goal of avoiding stray light on the science detector, while providing spectra in the wavelength range 370-960 nm with a resolving power that ranges from ~ 900 at 370 nm to ~ 200 at 960 nm. The signal to noise per resolution element obtained for a $V = 10$ magnitude star in a 1 minute integration varies between ~ 35 and 140. An analysis of the light curve constrains the radii of the planets relative to their parent stars' radii, which are, in turn, tightly constrained by the combination of absolute spectrophotometry and trigonometric parallaxes. The provisional optical design satisfies all the scientific requirements, including a $\sim 1\%$ rms flux calibration strategy based on observations of bright A-type stars and model atmospheres, allowing the determination of stellar angular diameters for nearby solar-like stars to 0.5%. This level of accuracy will be propagated to the stellar radii for the nearest stars, with highly reliable Hipparcos parallaxes, and more significantly, to the planetary radii.

KEYWORDS: Instrument optimisation; Optics; Space instrumentation; Spectrometers.

*Corresponding author: Carlos del Burgo (cburgo@uninova.pt)

Contents

1. Introduction	1
2. Science drivers and scientific requirements	3
3. Conceptual optical design	5
3.1 The telescope	6
3.2 The spectrograph optics	7
3.3 Data acquisition	9
4. Instrument performance	10
5. Absolute calibration	11
6. Summary	14

1. Introduction

The finding and characterisation of extrasolar planets is currently one of the most active research topics. Most discoveries of exoplanets come from the Doppler-wobble technique, which provides indirect evidence of the presence of a planet from the analysis of the periodic variations in the radial-velocity curve of a star, and allows the determination of $M_p \times \sin(i)$, where M_p is the planetary mass and i the inclination angle of the orbit. Transiting exoplanets are a subset of the exoplanets with $i \sim 90^\circ$ for which it is possible to constrain many of their properties. A planet transit causes a very small but revealing reduction in the apparent brightness of the host star. This dip in the host star's light curve (i.e., brightness as a function of time) allows one to determine the stellar density of the star and the physical parameters of the transiting planet, such as orbital radius and inclination, and more importantly, the radius of the planet (see, e.g., Seager & Mallén-Ornelas 2003). The period of the planet can also be derived when at least two consecutive transits are observed.

The accuracy in the determination of the properties of the planet from transit data critically depends on our knowledge of the properties of the star. For example, for a certain transit depth, the inferred planetary radius scales in proportion to the assumed stellar radius. Various methods have been used so far to determine the properties of stars with known transits (Torres, Winn & Holman 2008). For the stars with precise Hipparcos parallaxes¹ the determination of the stellar properties is relatively simple. When parallaxes are not available, the measurement and challenging interpretation of the depths and shapes of gravity-sensitive absorption features in the star's spectrum

¹The Gaia mission will increase by about four orders of magnitude the number of stars with accurate trigonometric parallaxes.

is usually considered as an alternative. It has been recently shown that the uncertainties can be significantly reduced by extracting the mean stellar density from the transit light curve (see Sozzetti et al. 2007 and Holman et al. 2007).

Transiting planets are much rarer than those found by the Radial Velocity (RV) technique, due to the statistically low probability of alignment required to produce a transit signature. The first planet found to transit was HD 209458b (Henry et al. 2000, Charbonneau et al. 2000), originally discovered by the RV technique. However, major recent efforts have made use of a range of wide angle time series surveys to discover transiting planets from the light curves of millions of stars (e.g., Horne 2003). Over 60 transiting extra-solar planets are currently known, most of them discovered by the projects WASP (Pollacco et al. 2006), HATNet (Bakos et al. 2004), OGLE (Udalski et al. 2002), and recently with the CoRoT mission (Auvergne et al. 2009). The most recent transit surveys have improved their detection algorithms and follow-up procedures, and therefore it is expected that transiting planet discoveries will number in the hundreds over the next few years.

Ground-based photometry is severely limited in precision by the scintillation noise resulting from air turbulence in the Earth’s atmosphere at altitudes of $\lesssim 4$ km. This noise is smaller for large telescope apertures, but even for the largest 10-m class ground-based facilities it is extremely difficult to obtain milli-magnitude (0.1%) sensitivity in short exposures. Another problem with ground-based observations is the provision of long-term (several days or weeks) monitoring of a target, due to the day-night cycle. Even with polar telescopes or a network of telescopes sited at different longitudes, the quality of the observations will nevertheless be highly variable due to changing weather conditions. Space-borne instruments offer a solution by moving above the atmosphere, even though the passage through the South Atlantic Anomaly (SAA), and solar eclipses by the Earth’s limb, may reduce the number of observations (see, e.g., Sirianni & Mutchler 2005). Much current and future investment and planning is being directed towards space-based facilities designed for, or capable of, searching for and studying transits, including CoRoT, Kepler, JWST and ESA’s planned Cosmic Vision mission Plato. These missions, though crucial, are extremely expensive. However, known transits are actually quite bright, and measurements can be made using far less ambitious instruments. Indeed, to fully study transiting planet populations in the future, a far more economical means of obtaining large amounts of space-based data will be preferred.

Over the last few years, the use of satellites with masses below 100 kg has become feasible, mainly due to improvements in the accuracy with which the satellites can point (Walker et al. 2003; Grillmayer, Falke & Roeser 2005; Grocott et al. 2006). Small, light satellites require much smaller launch vehicles than heavy satellites, which considerably reduces the cost of such missions. It is also possible for a microsatellite to “piggyback”, using spare payload space associated with larger satellite launches. An early trailblazer for such micro-satellite technology is the Canadian-led MOST project (Micro-variability and Oscillations of Stars, Walker et al. 2003), whose instrument is housed in a suitcase-sized micro-satellite (~ 60 kg) and was launched into low-earth sun-synchronous orbit (820 km altitude, 100 min period) in June 2003. For MOST orbit, high levels of cosmic rays due to the passage through the SAA and solar eclipses reduce the number of observations by ≈ 10 % (Walker et al. 2003, Miller-Ricci et al. 2008).

Ultra-precise space-based photometry provides the critical means to study known transiting planet systems in a wide variety of ways, both to better characterise and understand the transiting planets themselves, and also to search for evidence of additional planets with sensitivities reaching

down to the terrestrial planet range. There are different areas of research that can be considered, for example hunting for unseen planets with transit-timing (Agol et al. 2005; Holman & Murray 2005), terrestrial planet transits (e.g., Croll et al. 2007); detailed stellar properties through astero-seismology (Kjeldsen et al. 2008), planet albedos (Rowe et al. 2006, 2008), or moons and rings (Barnes & O’Brien 2002, Barnes & Fortney 2004).

Absolute spectrophotometry can be used to constrain stellar angular diameters more accurately than photometric data, and much more efficiently than interferometric measurements. An observatory in space could provide accurate stellar physical properties, such as angular diameters and effective temperatures, for a significant sample of bright stars with a modest time investment. These are fundamental measurements that are required not only to characterise orbiting planets but to derive other stellar properties such as ages. Currently, the only operational spectrophotometer in space suitable for accurate measurements of stellar fluxes over a wide wavelength range is the Hubble Space Telescope Imaging Spectrograph STIS. The vast costs of operating the Hubble Space Telescope plus the high demand for observing time make such a program with STIS unfeasible. A simpler instrument on a micro-satellite would provide similar or higher accuracy for bright sources at a small fraction of the costs.

We present a preliminary optical design for the instrument PHASES (Planet Hunting and AsteroSeismology Explorer Spectrophotometer) that aims at the determination of the stellar and planetary properties of nearby transiting systems with unprecedented precision. The telescope feeding PHASES has an aperture of 20 cm, which will make it possible to obtain spectra in the wavelength range between 370 and 960 nm with a resolving power of $R > 200$ and a signal-to-noise ratio per resolution element ranging from ≈ 35 to 140 in integration times of 1 minute, and achieve a photometric precision better than 10 ppm observing two planet transits of stars brighter than 10 mag in the Johnson V band (assuming a transit length of ≈ 4 hours). PHASES will also allow us to tightly constrain the properties of the parent stars, with the benefit of a better characterisation of the hosted planets. The total cost estimated for the entire project (design, manufacture, launch and operations) is about 6 million Euros, the launch being the most expensive component.

In this paper we outline the conceptual optical design of the telescope and spectrometer PHASES. The description of the microsatellite and the data handling (compression and download to ground stations) is beyond the scope of this paper. Here we highlight the crucial importance of determining the absolute flux level as accurately as possible to better determine the properties of the star and the associated planet. In order to achieve that, we have carefully developed an optical design that offers maximum control of the stray light. §2 presents the scientific motivation and requirements for PHASES. §3 is devoted to the preliminary optical design. §4 presents the predicted performance of PHASES, and §5 describes the flux calibration plan. Finally, §6 summarises the paper.

2. Science drivers and scientific requirements

PHASES’ main science driver is to dramatically improve our knowledge of known planetary systems around bright parent stars, which generally consist of a solar-like star with a close-in giant planet in orbit. The main objectives can be summarised:

- To determine with high precision the physical properties (effective temperature, surface gravity, mean density) of the parent stars from the analysis of their spectra and light curves (derived from the spectra themselves). The radii of the stars will be constrained from absolute fluxes and parallaxes.
- To study the seismic activity in the star from the corresponding variations in the light-curve.
- To determine the orbital properties (distance and inclination) and physical properties (radius and mass) of the planets with unprecedented precision from the corresponding periodic variations in the light-curve. A fortuitous discovery of Callisto-like moons might be possible if they eclipse the light from the parent stars at the time of the giant planet transit.

These science goals require spectrophotometry from space in order to improve upon the precision achieved for existing observations. Pre-transit and post-transit spectra will provide information about the properties and level of activity of the star. The spectral range will be from 370 to 960 nm, which contains many signatures to characterise the stellar properties, and also includes activity indicators such as the CaII H&K doublet. The blue part of the spectrum is highly valuable to constrain the star's surface gravity, mainly through the Balmer jump. A minimum resolving power of ~ 100 is required, but higher resolution will lead to better results.

The geometry of the transit can be determined from the light curve during the transit itself, and two consecutive transits make possible the determination of the period. To observe a transit produced by an Earth-like planet around a solar-like star requires a photometric precision of 80 ppm. Our scientific requirement is to achieve 10 ppm (goal: 3 ppm) for a $V=6$ mag solar-like star with a transit length of 3 hours. The square root of the transit depth corresponds to the ratio of the planetary and stellar radii. A precise determination of the planet radius depends on a previous accurate determination of the stellar radius, to be extracted from the comparison of the observed absolute stellar flux and theoretical fluxes at the stellar surface, and measured parallaxes. Standard plane-parallel model atmospheres can be combined with absolute spectrophotometry to constrain the stellar atmospheric parameters for dwarf stars, in order to assign an appropriate model atmosphere and theoretical fluxes.

We have carried out simulations of solar-like spectra assuming no interstellar extinction, a resolving power of 100 and a signal-to-noise ratio per resolution element of about 100. They show that for the spectral coverage provided by PHASES (370 – 960 nm), the stellar metallicity, effective temperature, and surface gravity of a solar-like star can be determined to within 0.2 dex, 50 K, and 0.3 dex, respectively. Using an independent determination of the metallicity from high-resolution spectroscopy, it is possible to constrain the effective temperature and the surface gravity of the star to better than 20 K, and 0.1 dex, respectively. An analysis of the solar fluxes compiled by Colina et al. (1996) using Kurucz (1993) model atmospheres leads to a solar angular diameter determination of 1928 ± 40 arcsec (1σ), only 0.5% larger than the value from astrometric measurements (see Table 2 of Golbasi et al. 2001, or Kuhn et al. 2004). Similar agreement is obtained in an analysis of the HST-STIS spectrum of Vega (Bohlin & Gilliland 2004), giving us confidence that the same accuracy would be attainable for stars in the A-F-G spectral type range.

Stellar radii can span a wide range in any given spectral class. The effect of metallicity is only secondary – a reduction of about 0.2 dex from $[\text{Fe}/\text{H}]=0$ to -1.5 for a solar-like star – and the

typical metallicity span of stars in the Galactic thin disk is about 0.2 dex. Much larger variations are found due to evolution as the stars leave the zero-age main sequence, especially once they exhaust the hydrogen in their cores and begin their ascent on the subgiant branch. Consequently the very precise radii measured in eclipsing binary systems show scatter in excess of 0.4 dex among unevolved (dwarf and subgiant) A and F-type stars with similar surface temperatures (see Fig. 2 of Andersen 1991, and also the luminosity spread in the Hipparcos field stars discussed by van Leeuwen 2009 and references therein). These variations can be constrained through spectroscopic determinations of the surface gravity, but for a typical accuracy of 0.1 dex in the surface gravity, the radius will be uncertain by 0.05 dex, or about 12%.

The sample of stars to be observed with PHASES would be compiled from the list published by The Extrasolar Planet Encyclopedia ². This list is periodically updated and it is expected that will be significantly enlarged in the next years. The typical periods of the nearby known exoplanets are a few days. We will select a sample of bright stars (V-band magnitude below 10 mag) that could be continuously observed during those periods (i.e, the stars are inside the Continuous Viewing Zone of the satellite; CVZ). Given the current list of bright stars, a CVZ with limiting declinations of 15° and 75° is appropriate. To observe the proposed CVZ the microsatellite carrying PHASES should be released into a low Earth (850 Km height) Sun-synchronous orbit with an inclination to the equator of 133°.

To determine the transit shape and extract most of the parameters of the star-planet system, a fast cadence is required, in addition to a high photometric precision. The determination of an appropriate optical observing strategy depends upon the detector read time and the telescope aperture. We discuss this issue further in Sect. 4.

3. Conceptual optical design

PHASES is designed to be carried on a microsatellite launched into low-earth-orbit. The microsatellite enclosure should contain a cubic science payload of 50-60 cm side, into which the telescope and the spectrograph have to be packed alongside the on-board electronics, computer, and power supply. Two of the primary mechanical design drivers will be pointing accuracy so that the science object can be acquired, and pointing stability to maintain stable illumination of the spectrograph. There are two independent detectors, one CCD for acquisition and tracking fed by the telescope and one for science in the spectrograph; both are to be passively cooled to just above the ambient temperature of the satellite, estimated to be ~ 220 K, and stabilised to $\sim 230 \pm 0.1^\circ$ K by heating elements on the CCD mounting plates (Walker et al. 2003). The science CCD in the spectrograph collects the spectrally dispersed light from the object of interest. The function of the tracking CCD is to acquire data for the guiding and pointing control. The tracking array is read out several times during each exposure of the spectrograph CCD and the centroids of all sources in the field of view are found. The comparison of the drift in the centroids between consecutive readouts is used to maintain the position of the science object on the slit via the satellite attitude control. In presenting the optical design it is assumed that the pointing accuracy will be 1'', which would meet the requirements. We first present the telescope optics and imaging on the tracking CCD, then the spectrograph optics.

²<http://exoplanet.eu/>

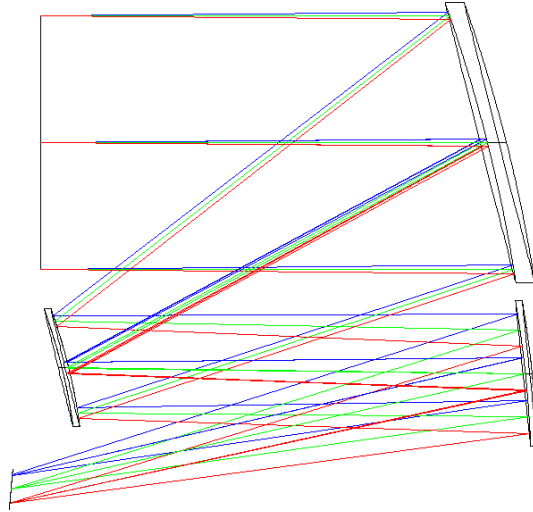


Figure 1. The optical layout of the modified Baker type telescope giving unobscured F5.2 imaging of the 1° field of view onto the tracking CCD. The three ray bundles focused onto the CCD are from sources at the centre and margins of the field of view. The enclosing box measures $30\text{ cm} \times 43.6\text{ cm} \times 23\text{ cm}$.

3.1 The telescope

Figure 1 presents the conceptual telescope layout. The design is of a modified Baker type, giving unobscured illumination of the 1024×1024 , $18\mu\text{m}$ pixel tracking CCD by the 1° square field of view. The aperture stop is 20 cm in diameter, and it is remote from the primary mirror. The choice of layout is driven by four considerations: packaging within the confines of the micro-satellite, control of stray light on the science detector, maximum light gathering, and image quality across the field.

A compactly folded, diffraction limited, telescope is chosen to permit the top of the micro-satellite to be used as an optical bench on which the telescope optics, tracking CCD and spectrograph are mounted, with the aperture stop located in the bench. All three mirrors are sized so that the mirrors for the qualification model, flight spare, flight model and one spare can be cut from a single parent. The specification of the aperture, field of view and pixel size determine the telescope F-number of 5.2, giving a plate scale of $195''\text{ mm}^{-1}$ on the tracking detector. The design is diffraction limited giving an angular diameter for the Airy disc of $0.92''$ at 370 nm and $2.38''$ at 960 nm. Distortion is low, reaching -0.014% at the edge of the field.

A graph of the diffraction ensquared energy is shown in Figure 2. The diffraction performance of the telescope is essentially constant over the whole field of view. The pixel scale means that the Airy disc of a point-like source will be $\sim 2/3$ pixels. Defocusing the images on the tracking CCD by displacing it $100\mu\text{m}$ would spread the image of a point source over two pixels. Since the purpose of the tracking CCD is for centroiding and not imaging this would be an acceptable practise giving more accurate centroids. This will be degraded by the fixed form errors and mounting tolerances of the three mirrors to give a Strehl ratio of about 80% in the flight model.

For the telescope, accurate centroiding over the full 1° field of view is the dominant requirement. Image quality is of critical importance at the spectrograph *slit*, where the smallest possible spread in the light spot is required. The spectrograph is to be fed by a pick-off mirror that will col-

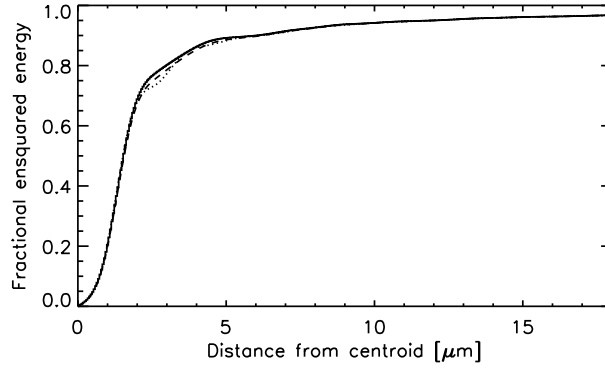


Figure 2. Diffraction ensquared energy: the performance is virtually identical across the entire field. Solid and dotted lines correspond to the polychromatic and diffraction limit cases, respectively. The image of a point-like source will be $\sim 2/3$ pixels. Displacing the tracking CCD by $100\ \mu\text{m}$ would spread the image of a point source over two pixels.

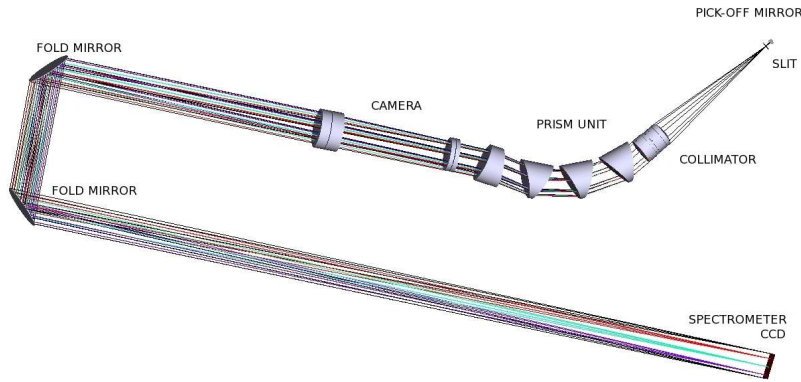


Figure 3. Provisional layout of the spectrograph. The telescope pupil is imaged onto the front surface of the prism by the collimating optics (not shown) and the spectrally dispersed object is anamorphically imaged onto the science CCD by the spectrograph camera, spreading the image over ten pixels in the spatial direction.

lect the science object image positioned at one corner of the tracking CCD. Positioning the pick-off at the corner minimises the obscuration of the tracking CCD, whilst allowing continuous tracking of the science object onto the spectrograph slit.

3.2 The spectrograph optics

The preliminary design of the PHASES spectrograph is shown in Figure 3. The pick-off mirror positions the point-like science object on the slit. The optics comprises a collimating lens corrected for secondary spectrum, prism unit, and camera; the whole being folded to fit into a space envelope measuring $28\text{ cm} \times 9\text{ cm} \times 4\text{ cm}$. The camera is F44, determined by the sampling requirement at the spectrograph CCD, the $18\ \mu\text{m}$ pixel size, and the telescope F-number. The tentative width of the slit is $8.2''$ – the diameter of the fourth minimum of the Airy pattern at 960 nm – with an aspect

ratio of three. A detailed study will be carried out from theoretical simulations and laboratory tests to determine the optimum width and length. The slit has to be sized to limit variations in the flux reaching the spectrograph detector due to pointing drifts, while permitting adequate control over stray light, and avoiding excessive sky background. The slit acts as a field stop and is the only port through which light may enter the spectrograph enclosure. For a 8.2×8.2 arcsec² square slit, the expected background, dominated by zodiacal light for most observations, is about $\approx 22 - 23$ mag arcsec⁻², or $\approx 10^{-4}$ times the flux expected for our faintest targets (see, e.g., the Cycle 17 HST-STIS Instrument Handbook³). There are no geocoronal emission lines in the spectral window considered for PHASES.

The obscuration of the tracking CCD by the pick-off mirror will affect approximately 150×150 pixels of a 1024×1024 pixel array. A pointing accuracy of $1''$ gives an image displacement of $8.46''$ on the science CCD, corresponding to ~ 2.4 pixels. Note that this is pointing accuracy, not pointing stability; at the current time the pointing stability requirement is yet to be determined and will be a design driver for the satellite control system. Pointing stability must be maintained over the maximum exposure time of 60 seconds. The final pointing stability requirement will be determined by the ratio of the F-number of the spectrograph camera to the F-number of the telescope and the required sampling and image stability at the spectrograph CCD. The requirement could be relaxed by reducing the field of view of the telescope, thus allowing an increase in the telescope F-number and a reduction in the magnification between the focal planes of the telescope and spectrograph.

The collimator images the telescope exit pupil onto the second prism where there will be a stop sized to match the spectrally dispersed image of the aperture in the optical bench. Primary control over stray light in the spectrograph will be achieved by baffles between the slit and the collimator. Additional baffling will be located around the spectrally dispersed beam between the camera and the CCD. The camera is designed to produce an anamorphic image of the star on the spectrograph CCD with the science object imaged as a ten pixel FWHM stripe transverse to the direction of spectral dispersion.

Although simulations indicate that a resolving power $R \simeq 100$ would suffice to meet the science objectives, a higher resolution will help to better constrain the atmospheric parameters and is therefore preferred. The provisional optical design is diffraction limited over the full spectral range (see Figure 4). At the red end of the spectrum imaging will be diffraction limited, at the blue end it will be pixel limited. The resolution that will be obtained in operation will be influenced by the pointing stability, wavefront error due to surface form errors in the optics, and pixelation. Since the image of the star will be diffraction limited in the red and the wavefront errors will be least in the red we estimate $R \approx 200$ at $\lambda = 960$ nm rising to $R \approx 500$ at $\lambda = 500$ nm. At the blue end of the spectrum wavefront errors will be greatest and imaging will be pixel limited and we estimate $R \approx 900$ at $\lambda 370$ nm. The actual resolution will be determined by laboratory tests.

The system throughput to the spectrograph CCD is estimated to be 50% at 370 nm, 62% at 400 nm, and 65% for 500 nm and above. The final transmission will be greatly influenced by the choice of coatings used, giving some freedom to bias the throughput towards one end of the spectrum. With a dielectric coating on the mirrors, the throughput of the telescope could be raised above 95%, and biasing the efficiency of the coatings on the spectrograph optics towards the blue

³http://www.stsci.edu/hst/stis/documents/handbooks/currentIHB/c06_exptime6.html

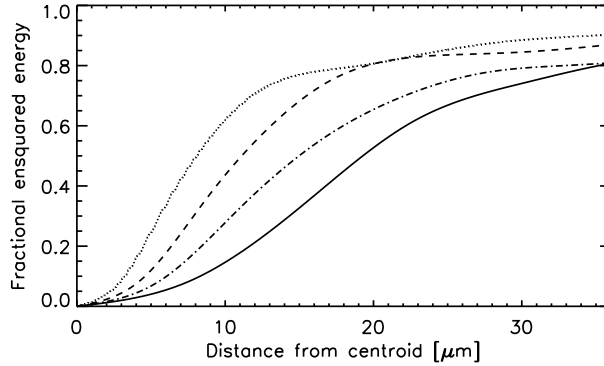


Figure 4. Diffraction ensquared energy of the spectrograph. The top lines corresponds to 370 nm, the lower lines to 550, 700 and 960 nm respectively. The Airy disc diameters are 2 pixels at 370 nm, 3 pixels at 500 nm, rising to 5.7 pixels at 960 nm.

can be used to partially offset the lower quantum efficiency of the detector. The final choice of coatings and glasses will be made later in the design cycle.

3.3 Data acquisition

The dispersed image of a star on the science detector or aperture will be sampled by 1024 pixels in the dispersion axis and 10 pixels in the perpendicular axis. The latter number may be modified according with current simulation and laboratory tests. The mean dispersion is $0.58 \text{ nm pixel}^{-1}$. The expected resolving power changes from ~ 900 at 370 nm to ~ 200 at 960 nm, which results in a higher resolution towards blue wavelengths, in line with the science needs.

The maximum exposure time is of 60 seconds, which allows us to obtain a minimum signal-to-noise per pixel of about 25 (i.e., 35 per resolution element at 370 nm) for the faintest ($V=10$) stars to be observed (see §4). The pixel binning strategy may be changed to optimize the observation of faint objects at lower resolving powers. A binning in the dispersion axis can be used to preserve the read noise per bin, increasing the signal-to-noise ratio.

The aperture (i.e. image of the spectrum on the CCD) should be defined, traced along the dispersion axis and extracted. It is required that the aperture of the same object may move only slightly during observations to reduce the impact of the pixel-to-pixel sensitivity variations in the detector on the determination of the small variations that are associated to the transit of a planet or the activity of a star.

A data reduction pipeline would be developed for PHASES, where problems such as the correction of cosmic rays, pointing instability and stray light subtraction will be sorted out (see, e.g., Huber & Reegen 2008). This would be discussed in a forthcoming publication once the simulations and laboratory tests of PHASES are completed. We highlight here that the use of spectrophotometry helps to clean up the images from cosmic rays, bad columns and dead pixels, since it is possible to make a comparison of the observed spectra with the state-of-the-art synthetic models, which mimic closely the observations (see Sect. 5). This is a significant advantage for performing ultra-precise measurements.

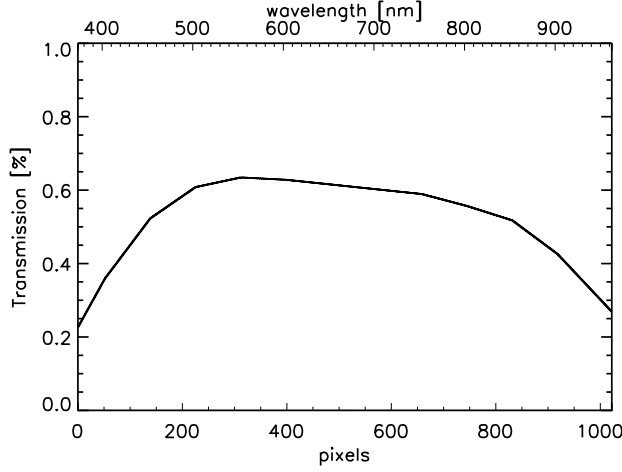


Figure 5. Predicted total transmission of PHASES versus wavelength.

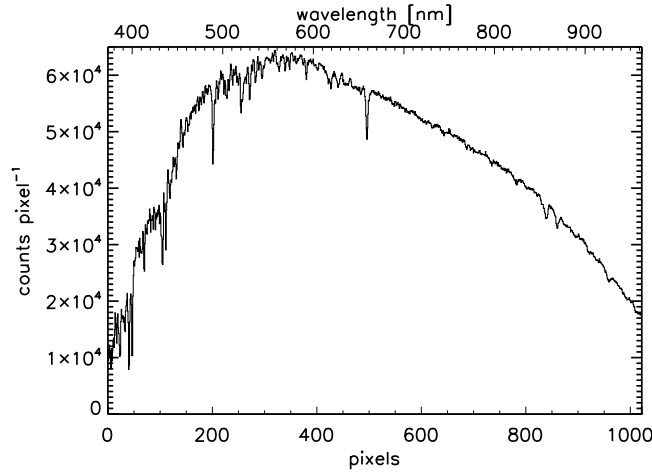


Figure 6. Spectral energy distribution prediction (in counts per photon) for the star HD 209458 as seen by PHASES with an exposure time of 60 seconds. Poisson noise has been added. Note the change in resolution from the blue to the red part of the spectrum

4. Instrument performance

The performance of PHASES has been estimated assuming that the telescope mirror transmission and the spectrograph specifications are as given in Sect. 3. The assumed quantum efficiency of the science detector is $\approx 40\%$ at 370 and 960 nm, with a maximum approaching $\sim 97\%$ at 550 nm, and values higher than 90% in the wavelength range between 480 and 750 nm. These capabilities can be provided by commercial back-illuminated deep depletion silicon CCDs (see, e.g., <http://www.e2v.com>). Fig. 5 shows the total predicted throughput as a function of wavelength and position on the chip.

The scientific requirement is to achieve a photometric precision of 10 ppm (goal: 3 ppm) using the full spectral range of PHASES for a $V=6$ mag solar-like star with a transit length of 3 hours. Our simulations show that it is possible to reach a photon-noise-limited precision of 2 ppm given the expected performance of PHASES. The only source of noise considered here is shot noise that is given by the square-root of the number of photons (assuming a gain of 1 count per photo-electron) and follows a Poisson distribution. The expected dark signal ($\leq 0.01 \text{ e}^- \text{ s}^{-1} \text{ pixel}^{-1}$) and read noise ($\leq 5 \text{ e}^-$) of the detector will be negligible for the full sample of interest in the typical exposure times.

The quality of acquired data will be degraded by satellite pointing jitter, pixel-to-pixel variations, dead or hot pixels and bad columns. These defects will adversely influence our ability to isolate variations intrinsic to the star (e.g., stellar activity) or due to planetary transits. The study of the influence of these effects, and their mitigation, will be the subject of a future report.

HD 209458 (G0V, $V=7.65$) is the brightest star with a known planet in orbit. For this object, a photon-noise-limited photometric precision of 5.7 ppm would be achievable in the 3.7 hour duration of the transit of planet HD 209458b. With two transits it would be possible to achieve a precision of 4.0 ppm. Fig. 6 shows a simulation of an observed spectrum (once the aperture has been extracted and spectrally calibrated) of the star HD 209458. Note how the resolution decreases from the blue to the red wavelengths. The minimum signal-to-noise per pixel for a single 1-minute spectrum of HD 209458 varies from ~ 70 at 370 nm to ~ 225 at about 960 nm. The signal-to-noise per resolution element is ≈ 100 at 370 nm and ≈ 380 at 960 nm. The star XO-3 with a V-band magnitude of 9.8 and a planet transit (Johns-Krull et al. 2007) that lasts 3.7 hours is as bright as the faintest stars intended to be observed, with an expected photon-noise-limited photometric precision of 10.9 ppm after two transits. A single 1 minute spectrum of XO-3 has a signal-to-noise per pixel that varies from ~ 25 at 370 nm to ~ 85 at 960 nm, with a maximum of 80 at 500 nm. The signal-to-noise per resolution element is ~ 35 at 370 nm, 130 at 500 nm and 140 at 960 nm.

5. Absolute calibration

The accuracy of the inferred planetary radius will depend upon the accuracy of the stellar radius; it is necessary to precisely characterise the parent star in order to characterise its planets. Stellar angular diameters can be determined from interferometry or by comparing predicted fluxes at the stellar atmosphere with those observed from Earth (provided an accurate flux calibration). With accurate angular diameters and distances (trigonometric parallaxes from Hipparcos/Gaia), we can determine accurately the properties of the parent stars.

There are two distinct methodologies for performing spectrophotometric calibration of astronomical observations. Most catalogues of spectrophotometric standards are derived from ground-based observations, carefully tied to absolute fluxes from a controlled source (see, e.g., Hayes 1985).

Alternatively, the spectrophotometric catalogue of the HST (FOS, STIS and NICMOS; see Bohlin 2007 and references therein) establishes the relative spectral energy distribution for a number of standards using a different strategy, based on theoretical, model-atmosphere, predictions. The absolute zero point of the HST scale is ultimately tied to the Vega V-band magnitude (see Colina & Bohlin 1994, Bohlin & Gilliland 2004, and references therein). The HST primary standards,

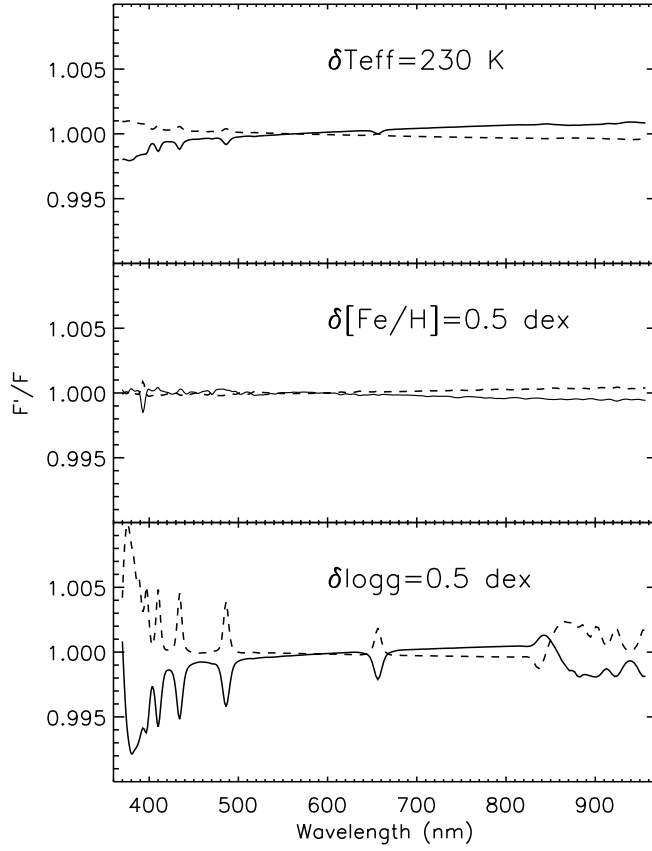


Figure 7. Relative variations in the stellar flux emerging from a Vega-like star associated with changes in the atmospheric parameters of $\delta T_{\text{eff}} = \pm 230$ K (upper panel), $\delta [\text{Fe}/\text{H}] = \pm 0.5$ dex (middle panel), and $\delta \log g = \pm 0.5$ dex (bottom panel). The solid lines correspond to the ratio between the flux after a reduction in one of the parameters and the original flux, while the dashed lines correspond to positive increments in one of the parameters.

for which the spectral shape is postulated based on model atmospheres, are three DA white dwarfs. Their atmospheric parameters (surface gravity and temperature) are defined from the analysis of the shape of the Hydrogen lines, which are highly sensitive to both the electron density (related to temperature) and the gas pressure (which correlates with the surface gravity). HST is free of atmospheric extinction, and the degradation of the charge transfer efficiency in its CCD's has been studied in detail (Goudfrooij et al. 2006).

This second approach relies on the premise that the atmospheres of these objects, made of pure hydrogen, are simple enough to model with high accuracy. With three white dwarf stars (G 191 B2B, GD 153 and GD 71), Bohlin reports an internal consistency at a level of $< 0.5\%$ for STIS (near-UV and optical), and about 1% for NICMOS observations (IR). The STIS spectrum of Vega (Bohlin & Gilliland 2004), calibrated upon the DA white dwarfs, closes the loop. A model atmosphere for this star matches the observations to 1–2 %, and a satisfactory agreement is also

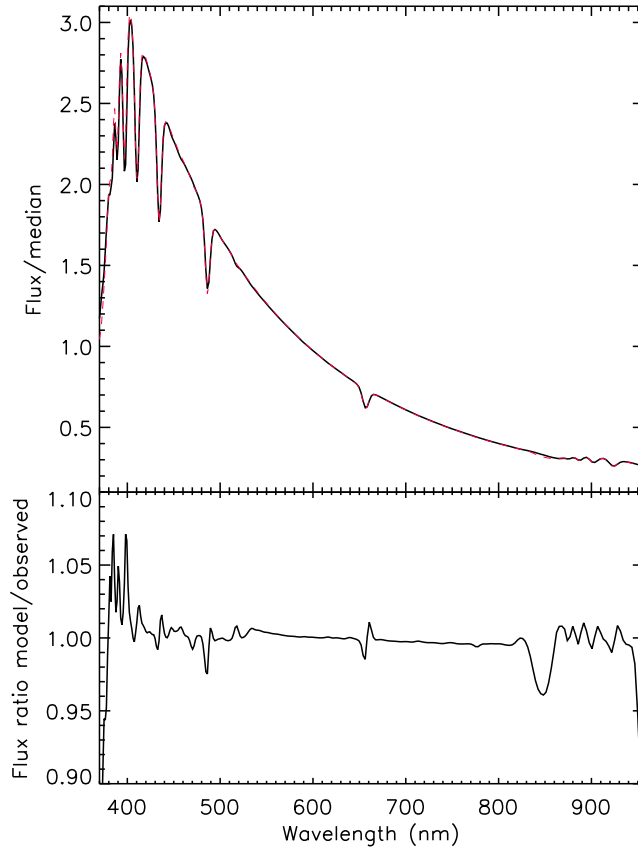


Figure 8. Vega fluxes in the PHASES spectral window normalized by their median value. All lines are for a resolving power of $R = 100$. The black solid and red broken lines in the upper plot show the observed spectrum (HST/STIS; Bohlin & Gilliland 2004) and the best-fitting model, respectively. The lower panel shows the ratio of the two.

found with the absolute fluxes of Hayes (Bohlin 2007).

The HST primary standards are too faint for a small aperture telescope like the one coupled to PHASES; The HST DAs are among the brightest white dwarfs known. Other DA could be analysed spectroscopically and used as standards, but there are none brighter than $V < 9.5$, and therefore they are unsuitable for PHASES.

The success in matching Vega’s spectrum with models found by Bohlin, suggests that A-type stars could also be used as standards. A-type stars have their continuum shaped by bound-free (photoionization) of neutral hydrogen atoms. Their atmospheric opacity is significantly affected by metal lines in the UV, but that is not the case for the optical and near-IR. In addition, at high-enough temperatures the vast majority of the electrons in these atmospheres are coming from the ionization of hydrogen. Furthermore, with lower densities than in white dwarfs, convection (an important source of uncertainty in the models) is inhibited at lower temperatures.

The published values for the temperature of Vega show a maximum range of about 230 K

(see García-Gil et al. 2006), and the surface gravity of any bright A-type star with trigonometric parallaxes from Hipparcos should be known to better than 0.2 dex. Fig. 7 illustrates that such a range in T_{eff} , as well as very large variations of 0.5 dex in $[\text{Fe}/\text{H}]$ or $\log g$, have only a very limited effect on the predicted fluxes over the spectral range of PHASES. The effect of metallicity, which should be possible to determine from existing (or easily obtained) ground-based high-resolution spectra to within ~ 0.1 dex, is, in fact, completely negligible. Consequently, bright A-type stars will be suitable for flux calibration of PHASES.

Given the extremely low sensitivity of the continuum to metallicity, we have attempted to determine T_{eff} and $\log g$ (fixing the metallicity) from the STIS spectrum of Vega smoothed to $R=100$, similar to the experiments described in §2 for the solar spectrum. The result is illustrated in Fig. 8, and the agreement is excellent with an RMS scatter of just 0.6% between 400 and 800 nm. We note that Vega is known to be a fast rotator (see, e.g., Aufdenberg et al. 2006), although this has a very limited impact in the PHASES wavelength range.

With an RMS scatter of 0.012 (1.2%), which we find when matching the solar spectrum with calculations based on Kurucz models (see §2), and 2–3 pixels per resolution element, the scaling factor between the computed and observed fluxes can be determined to ~ 0.1 %. Thus, the limiting factor for absolute calibration will be the zero point. If the calibration is anchored to Vega’s fluxes, this is given by the uncertainty in its $V = 0.026 \pm 0.008$ mag (Bohlin 2007). Our best fitting model ($[\text{Fe}/\text{H}] = -0.7$, imposed; $T_{\text{eff}} = 9506 \pm 23$ K; $\log g = 4.01 \pm 0.02$ dex) predicts a flux of $5.40 \times 10^7 \text{ erg s}^{-1} \text{ cm}^{-2} \text{ \AA}^{-1}$ at 555 nm, or, scaled by the inferred angular diameter ($\theta = 3.31$ mas), $3.48 \times 10^{-9} \text{ erg s}^{-1} \text{ cm}^{-2} \text{ \AA}^{-1}$ at 555 nm at Earth. This result is in excellent agreement with the figures from the STIS observations provided by Bohlin of $3.46 \times 10^{-9} \text{ erg s}^{-1} \text{ cm}^{-2} \text{ \AA}^{-1}$.

Provided the uncertainties in the atmospheric parameters for the calibration stars are comparable to those we inferred for the Sun or Vega, they will have a minor impact on the predicted fluxes. If the accuracy in the flux calibration is translated to the PHASES targets undisturbed by frequent observations of the standards, then such observations have the potential to lead to measurements of the angular diameter of the targets to a ~ 1 % level. This figure compares favourably to (model-based) photometric calibrations (Ramírez & Meléndez 2005; Casagrande 2008), or even interferometric measurements for most dwarfs (see, e.g., Baines et al. 2009). For bright stars with accurate parallaxes, we can expect the uncertainty in the estimated angular diameter to be retained in the implied radii to be used to derive the planets radii.

6. Summary

In this paper, we have outlined the motivation and concept for the PHASES instrument, which is designed to perform ultra-precise relative photometry and absolute spectrophotometry from a small-sized space platform. PHASES is optimised to provide a detailed characterisation of the transiting planets in orbit around nearby stars.

The proposed instrument has a dual objective: to measure the light curves of the target systems (stars brighter than $V=10$) during the transits with a precision better than $\sim 10^{-5}$ (10 ppm), and to obtain spectrophotometry of the parent star with an absolute accuracy of $\sim 1\%$. These two measurements, together with absolute parallaxes available from Hipparcos and later Gaia, can place tight constraints on the orbital elements and the radius of the transiting planet. The goals can be

realised by an opto-mechanical design optimised to control scattered light, by dispersing the target’s light over a large area of the detector, and minimising the cross-contamination of the spectrum by nearby sources. The avoidance of spectral cross-contamination is a critical driver for both the optical and the mechanical designs. This consideration leads to the adoption of an unobscured quasi-Baker telescope design, and the use of the slit as a spacial filter separating the acquisition and guiding function of the telescope optics from the spectrograph optics. Within the spectrograph enclosure, careful attention can be given to stray light control.

We argue that bright A-type stars can be used for flux calibration in the same way that DA white-dwarfs are used for fainter sources in many space-based instruments; by using model atmospheres and scaling the fluxes using broad-band photometry.

For solar-like stars, by determining the metallicity of the parent star using high-resolution spectroscopy, it is then possible to use $R \geq 100$ spectrophotometry to tightly constrain the effective temperature and the surface gravity. Assuming model atmospheres match the spectral energy distribution of real stars to better than 1 %, having absolute fluxes accurate to ~ 1 % will directly provide $\sim 0.5\%$ angular diameters and, for nearby stars, a similar accuracy in the stellar radius. It has been demonstrated that space-based light curves can be used to determine the stellar density and the ratio of the planetary to the stellar ratio with high precision (see, e.g. Seager & Mallén-Ornellas 2003, Mandel & Agol 2002), and therefore the availability, from a single instrument, of the two measurements, will lead to a significant improvement in the final accuracy of the inferred planetary radii, and the properties of the planetary systems in general.

Acknowledgments

The authors would like to thank David Pinfield and Dave Walton for useful discussions, and an anonymous referee for thoughtful comments.

References

- [1] E. Agol, et al., *On detecting terrestrial planets with timing of giant planet transits*, *Monthly Notices of the Royal Astronomical Society* **359** (2005) 567.
- [2] J. Andersen, *Accurate masses and radii of normal stars*, *Astronomy and Astrophysics Review* **3** (1991) 91.
- [3] J. P. Aufdenberg, et al., *First results from the CHARA array. VII. Long-baseline interferometric measurements of Vega consistent with a pole-on, rapidly rotating star*, *The Astrophysical Journal* **645** (2006) 664.
- [4] M. Auvergne, et al., *The CoRoT satellite in flight: description and performance*, *Astronomy and Astrophysics* **506** (2009) 411.
- [5] G. Á. Bakos, R. W. Noyes, G. Kovács, K. Z. Stanek, D. D. Sasselov, I. Domsa, *Wide-Field Millimagnitude Photometry with the HAT: A Tool for Extrasolar Planet Detection*, *The Publications of the Astronomical Society of the Pacific* **116** (2004) 266.
- [6] E. K. Baines, H. A. McAlister, T. A. Ten Brummelaar, J. Sturmann, L. Sturmann, N. H. Turner, S. T. Ridgway, *Eleven exoplanet host star angular diameters from the Chara array*, *The Astrophysical Journal* **701** (2009) 154.

- [7] J. Barnes, J. Fortney, *Transit detectability of ring systems around extrasolar giant planets*, *The Astrophysical Journal* **616** (2004) 1193.
- [8] J. Barnes, D. O'Brien, *Stability of satellites around close-in extrasolar giant planets*, *The Astrophysical Journal* **575** (2002) 1087.
- [9] R. C. Bohlin, *HST stellar standards with 1% accuracy in absolute flux*, in proceedings of *The Future of Photometric, Spectrophotometric and Polarimetric Standardization*, ASP Conference Series **364** (2007) 315.
- [10] R. C. Bohlin, R. L. Gilliland, *Hubble space telescope absolute spectrophotometry of Vega from the far-ultraviolet to the infrared*, *The Astronomical Journal* **127** (2004) 3508.
- [11] L. Casagrande, *Infrared flux method and colour calibrations*, *Physica Scripta* **133** (2008) 014020.
- [12] D. Charbonneau, et al., *Detection of planetary transits across a sun-like star*, *The Astrophysical Journal* **529** (2000) L45.
- [13] L. Colina, R. C. Bohlin, *Absolute flux calibration of optical spectrophotometric standard stars*, *The Astronomical Journal* **108** (1994) 1931.
- [14] L. Colina, R. C. Bohlin, F. Castelli, *The 0.12-2.5 micron absolute flux distribution of the sun for comparison with solar analog stars*, *The Astronomical Journal* **112** (1996) 307.
- [15] B. Croll et al., *Looking for super-earths in the HD 189733 system: a search for transits in MOST space-based photometry*, *The Astrophysical Journal* **671** (2007) 2129.
- [16] P. Goudfrooij, R. C. Bohlin, J. Maíz-Apellániz, R. A. Kimble, *Empirical Corrections for Charge Transfer Inefficiency and Associated Centroid Shifts for STIS CCD Observations*, *The Publications of the Astronomical Society of the Pacific* **118** (2006) 1455.
- [17] D. Huber, P. Reegen *A MOST open-field data reduction software and its applications to BRITe Communications in Asteroseismology*, **152** (2008) 77.
- [18] A. García-Gil, R. J. García López, C. Allende Prieto, I. Hubeny, *A study of the near-ultraviolet spectrum of Vega*, *The Astrophysical Journal* **623** (2005) 460.
- [19] O. Golbasi, F. Chollet, H. Kiliç, V. Sinceac, A. Aslan, E. Sozen, *Solar radius determinations obtained with the CCD astrolabe at TUBITAK National Observatory*, *Astronomy and Astrophysics* **368** (2001) 1077.
- [20] D. Green, J. Matthews, S. Seager, R. Kuschnig, *Scattered light from close-in extrasolar planets: prospects of detection with the MOST satellite*, *The Astrophysical Journal* **597** (2003) 590.
- [21] G. Grillmayer, A. Flake, H. -P. Roeser, *Technology Demonstration with the Micro-Satellite Flying Laptop, Small Satellites for Earth Observation - Selected Proceedings of the 5th International Symposium of the International Academy of Astronautics*, ISBN 978-3-11-018851-6, Berlin, Germany (2005) 419-427
- [22] S. C. O. Grocott, R. E. Zee, G. J. Wells, R. Wessels, A. Beatties, S. Park, *Expanding the Capabilities of the MOST Spacecraft*, *ASTRO 2006 - 13th CAI Canadian Astronautics Conference*, Montreal, Canada, April (2006)
- [23] G. W. Henry, G. W. Marcy, R. P. Butler, S. S. Vogt, *A transiting "51 Peg-like" planet*, *The Astrophysical Journal* **529** (2000) L41.
- [24] D. S. Hayes, *Stellar absolute fluxes and energy distributions from 0.32 to 4.0 microns*, in proceedings of the IAU Symposium No. 111 *Calibration of Fundamental Stellar Quantities* **111** (1985) 225-249; Discussion, p. 250-252.

- [25] M. J. Holman, et al., *The Transit Light Curve (TLC) Project. VI. Three Transits of the Exoplanet TrES-2*, *The Astrophysical Journal* **664** (2007) 1185.
- [26] M. J. Holman, N. W. Murray, *The use of transit timing to detect terrestrial-mass extrasolar planets*, *Science* **307** (1288) .
- [27] K. Horne, *Status and prospects of planetary transit searches: hot jupiters galore*, *ASP Conference Series* **294** (2003) 361.
- [28] C. Johns-Krull, et al., *The Unusual Transiting Extra-Solar Planet Orbiting XO-3* *Bulletin of the American Astronomical Society* **38** (2007) 225.
- [29] H. Kjeldsen, et al., *The Amplitude of solar oscillations using stellar techniques*, *The Astrophysical Journal* **682** (2008) 1370.
- [30] J. R. Kuhn, R. I. Bush, M. Emilio, P. H. Scherrer, *On the Constancy of the Solar Diameter. II.*, *The Astrophysical Journal* **613** (2004) 1241.
- [31] R. L. Kurucz, *Stellar atmosphere programs and 2 km/s grid*, *SAO, Kurucz CD-ROM* **13** (1993).
- [32] F. van Leeuwen, *Parallaxes and proper motions for 20 open clusters as based on the new Hipparcos catalogue*, *Astronomy and Astrophysics* **497** (2009) 209.
- [33] K. Mandel, E. Agol, *Analytic light curves for planetary transit searches*, *The Astrophysical Journal* **580** (2002) L171.
- [34] M. S. Marley, et al., *Reflected spectra and albedos of extrasolar giant planets. I. Clear and cloudy atmospheres*, *The Astrophysical Journal* **513** (1999) 879.
- [35] E. Miller-Ricci, et al., *MOST Space-based Photometry of the Transiting Exoplanet System HD 209458: Transit Timing to Search for Additional Planets*, *The Astrophysical Journal* **682** (2008) 586.
- [36] I. Ramírez, J. Meléndez, *The effective temperature scale of FGK stars. I. Determination of temperatures and angular diameters with the infrared flux method*, *The Astrophysical Journal* **626** (2005) 446.
- [37] J. F. Rowe, et al. 2006, *An upper limit on the albedo of HD 209458b: direct imaging photometry with the MOST satellite*, *The Astrophysical Journal* **646** (2006) 1241.
- [38] D. Pollacco, et al. 2006, *The WASP Project and the SuperWASP Cameras*, *The Publications of the Astronomical Society of the Pacific* **118** (2006) 1407.
- [39] J. F. Rowe, et al., *The very low albedo of an extrasolar planet: MOST space-based photometry of HD 209458*, *The Astrophysical Journal* **689** (2008) 1345
- [40] S. Seager, G. Mallén-Ornelas, *A Unique Solution of Planet and Star Parameters from an Extrasolar Planet Transit Light Curve*, *The Astrophysical Journal* **585** (1003) 1038.
- [41] M. Sirianni, M. Mutchler, *Radiation Damage in HST, Scientific Detector for Astronomy 2005* Springer Netherlands, ISBN: 978-1-4020-4330-7 (2006) 171-178
- [42] A. Sozetti, G. Torres, D. Charbonneau, D. W. Latham, M. J. Holman, J. N. Winn, J. B. Laird, F. T. O'Donovan, *Improving stellar and planetary parameters of transiting planet systems: the case of TrES-2*, *The Astrophysical Journal* **664** (2007) 1190.
- [43] G. Torres, J. N. Winn, J. M. Holman, *Improved parameters for extrasolar transiting planets*, *The Astrophysical Journal* **677** (2008) 1324.

- [44] A. Udalski, B. Paczynski, K. Zebrun, et al., *The Optical Gravitational Lensing Experiment. Search for planetary and Low-Luminosity Object Transits in the Galactic Disk. Results of 2001 Campaign*, *Acta Astronomica* **52** (2002) 1.
- [45] G. Walker, et al., *The MOST asteroseismology mission: ultraprecise photometry from space*, *Publications of the Astronomical Society of the Pacific* **115** (2003) 1023.